Transducer resolution and the turbulent wall pressure spectrum

Richard M. Lueptow
Department of Mechanical Engineering, Northwestern University, Evanston, Illinois 60208

(Received 26 July 1993; revised 27 July 1994; accepted 17 August 1994)

The size of a pressure transducer will affect the accuracy of measurements of the wall pressure beneath a turbulent boundary layer because of spatial averaging over the sensing area of the transducer. The effect of transducer size on the wall pressure spectrum was investigated by numerically applying wave-number filters corresponding to various size and shape transducers to a database of wall pressure generated from a direct numerical simulation of turbulent channel flow. Circular transducers with piston-type and deflection-type sensitivities were modeled along with square transducers having piston-type sensitivity. The rms wall pressure is attenuated less for a deflection-type transducer than for a piston-type transducer of the same area. The wave-number spectrum of the wall pressure measured using a large transducer has lobes and zeros corresponding to those in the wave-number response function of the transducer. These lobes and zeros in the wave-number spectrum are also evident in the frequency spectrum, although they are smeared. Using Taylor's frozen field hypothesis, an approximate upper bound on the frequency of wall pressure fluctuations that can be measured before the zeros in the wave-number response function is $\omega d/U_c < C$, where ω is the frequency, d the dimension of the transducer, U_c the convection velocity, and C 6.3, 7.7, and 11.0 for square piston, circular piston, and circular deflection transducers, respectively. The Corcos correction to the wall pressure spectrum recovers the true spectrum within this bound.

PACS numbers: 43.60.Cg, 43.30.Xm, 47.27.Nz

INTRODUCTION

The pressure fluctuations at the wall beneath a turbulent boundary layer are the result of the integral effect of fluctuations in the velocity field. The size of a wall pressure transducer limits the accuracy of measurements of the fluctuating wall pressure because spatial averaging over the face of the transducer effectively low-pass filters the signal. As a result, small transducers are more accurate than large transducers in measuring wall pressure fluctuations.

The problem of spatial resolution has been addressed both theoretically and experimentally.[1] Corcos[2–4] estimated the attenuation resulting from the finite size of the wall pressure transducer with a uniform sensitivity across its sensing surface for both circular and square transducers using a model that separates the streamwise and spanwise dependence of the cross-spectral density of the wall pressure. The amplitudes of the one-dimensional cross-spectral density functions were based on measurements of the wall pressure field.[5] Corcos' scheme has been used extensively to correct wall pressure frequency spectra. Although Willmarth and Roos[6] questioned the validity of the Corcos correction, the Corcos model was recently reexamined in the wave-number domain.[7] The attenuation predicted by the wave-number model matched that of Corcos quite well. White[8] and Kirby[9] extended Corcos' analysis to elliptical, rectangular, fish-shaped, and diamond-shaped transducers with uniform sensitivity. The Corcos correction method has been used to develop a correction for a hydrophone based on its experimentally measured sensitivity.[10] Chase[11] considered the effect of nonuniform sensitivities and transducer shapes on different portions of the wave-number spectrum of the wall pressure. Ffowcs-Williams[12] extended the Corcos and Chase theories to include constraints in the low-wave-number portion of the wall pressure spectrum for a transducer with uniform sensitivity. In spite of these attempts to modify the Corcos theory, the original Corcos model[3] is most commonly used to correct experimental wall pressure spectra.

The effect of transducer resolution on the measurement of the wall pressure has been studied experimentally as well. Geib[13] devised a scheme using a pair of microphones of different sizes but with similar spatial sensitivity that was capable of experimentally correcting the attenuation of the wall pressure spectrum resulting from spatial averaging. Bull and Thomas[14] measured the attenuation resulting from spatial averaging over the face of the transducer and found that the transducer size directly affects the measured rms wall pressure, although the effect of the Reynolds number cannot be neglected.[15] Schewe[16] measured the frequency spectrum of the wall pressure using microphones of different sizes and found that most of the attenuation in the rms wall pressure results from loss of transducer response at high frequencies. Nevertheless, a transducer with diameter $d_+ = 19$ was adequate to resolve the essential scales of the wall pressure fluctuations. (The + subscript denotes scaling with the kinematic viscosity ν and the friction velocity U_τ.) Schewe used the Corcos correction to account for the attenuation resulting from spatial averaging. While the Corcos correction worked reasonably well for $d_+ < 160$, the correction was inadequate for larger transducers.

Although d_+ has typically been the parameter used to quantify the spatial resolution of a wall pressure transducer, Keith *et al.*[17] showed that it is not the only appropriate measure of the transducer size. Using dimensional analysis, they

 0001-4966/95/97(1)/370/9/$6.00

TABLE I. Parameters of the direct simulation database (see Refs. 18–20).

$Re_\delta = U_{cl}\delta/\nu = 3200$			
$Re_\theta = U_{cl}\theta/\nu = 280$			
$Re_\tau = U_\tau\delta/\nu = 180$			
Streamwise: $L_x/\delta = 4\pi$	$N_x = 128$	$\Delta x_+ = 17.6$	$L_{x+} = 2253$
Wall normal: $L_y/\delta = 2$	$N_y = 129$	$\Delta y_+ = 0.05$ (near wall) to $\Delta y_+ = 4.4$ (centerline)	
Spanwise: $L_z/\delta = 4\pi/3$	$N_z = 128$	$\Delta z_+ = 5.9$	$L_{z+} = 755$
$\Delta t U_\tau/\delta = 3.75\times10^{-3}$			

reasoned that the spatial resolution parameter depends upon the scaling used to present the wall pressure spectrum. For wall pressure spectra scaled using an inner scaling, based on the near wall scales of the friction velocity and the kinematic viscosity, the correct parameter is $d^* = d_+(U_\tau/U_{cl})$, where U_{cl} is the centerline or free-stream velocity. For an outer scaling, based on the free-stream velocity and an integral length scale such as the displacement thickness δ^*, the correct parameter is d/δ^*. They also noted that using spectral correction procedures such as the Corcos correction cannot fully recover the true spectrum.

The availability of a numerical database for turbulent channel flow[18] allows the analysis of the problem of spatial resolution of wall pressure transducers in a controlled setting. Quite simply, wall pressure transducers of different sizes, shapes, and sensitivities can be applied numerically to the database and the resulting wall pressure spectrum calculated. The goal of this work was to determine the effect of transducer spatial resolution on a known, computationally derived wall pressure field by applying the spatial filtering characteristics of circular and square transducers of several different sizes. Furthermore, the Corcos method was used to correct the spectra to determine the effectiveness of this commonly used method for a known wall pressure field.

I. SPATIAL AVERAGING IN THE NUMERICAL DATABASE

A direct numerical simulation of turbulent channel flow, described in detail by Kim *et al.*,[18] was used to generate the pressure statistics presented in this paper. This database is the same as that used by Kim[19] and Choi and Moin[20] for analysis of the structure and space-time characteristics of turbulent wall pressure fluctuations. It is based on the direct solution of the Navier–Stokes equations using a spectral method for spatial derivatives and time advancement by a semi-implicit scheme.[18] The computational domain for the simulation is $L_x\times L_y\times L_z$ of $4\pi\delta\times2\delta\times(4\pi/3)\delta$ in the streamwise x, wall-normal y, and spanwise z directions, where δ is the half-channel width. The streamwise and spanwise boundary conditions are periodic. The number of grid points N and other details of the computational domain and flow parameters are provided in Table I. The simulation was carried out for 25 640 time steps, saving the pressure for the entire plane of one of the walls at every tenth step corresponding to $\Delta t = 0.0667\ \delta/U_{cl}$.

The circular and square pressure sensors that were modeled were assumed to respond instantaneously in time. Uniform sensitivity and deflection-type sensitivity were considered for circular sensors, while only uniform sensitivity was considered for square sensors. Uniform sensitivity transducers have an invariant sensitivity across the entire sensing surface of the transducer. This model reflects the sensitivity of ceramic piezoelectric transducers. The sensitivity of a deflection-type sensor is modeled by the first mode of vibration of a membrane. This sensitivity distribution is typical of condenser microphones and some hydrophones.[21] Pinhole microphones, often used because of their small size, have a nonuniform sensitivity, but it is not necessarily that of a deflection-type transducer.[22]

The normalized wave-number response function $H(\mathbf{k})$ for a circular transducer of radius r_0 with uniform sensitivity is

$$H(\mathbf{k}) = \frac{2J_1(kr_0)}{kr_0}, \tag{1}$$

where $k = (k_x^2 + k_z^2)^{1/2}$ is the modulus of the wave number $\mathbf{k}$ with streamwise component k_x, and spanwise component k_z, and J_1 the Bessel function of order one.[21] The wave number k_0 corresponding to the first zero of the normalized wave-number response for a circular piston transducer satisfies $k_0 r_0 = 3.832$. A circular deflection sensor of radius r_0 has a normalized wave-number response of

$$H(\mathbf{k}) = \frac{a^2 J_0(kr_0)}{a^2 - (kr_0)^2}, \tag{2}$$

where J_0 is the Bessel function of order zero, and $a = 2.405$ so that $J_0(a) = 0$.[21] The wave number corresponding to the first zero of the normalized wave-number response for a circular deflection transducer occurs at $k_0 r_0 = 5.520$. A square transducer of side L with a uniform sensitivity has a normalized wave-number response function[21] of

$$H(\mathbf{k}) = \left(\frac{\sin(k_x L/2)}{k_x L/2}\right)\left(\frac{\sin(k_z L/2)}{k_z L/2}\right). \tag{3}$$

The first zero of the response occurs where $k_{0x}L = 2\pi$ or $k_{0z}L = 2\pi$.

The transducer response was modeled using spatial filtering in the wave-number domain. First, a two-dimensional Fourier transform[23] was applied to the pressure at the wall $P(x,z,t)$ for a particular time step t to convert the pressure into the wave-number domain $\mathbf{P}(k_x,k_z,t)$. The spatially filtered wave-number Fourier transform $\mathbf{P}'(k_x,k_z,t)$ was found using the normalized wave-number response

$$\mathbf{P}'(k_x,k_z,t) = H(k_x,k_z)\mathbf{P}(k_x,k_z,t). \tag{4}$$

A two-dimensional inverse Fourier transform was applied to $\mathbf{P}'(k_x,k_z,t)$ to transform the spatially filtered data back into the space domain to obtain the filtered wall pressure $P'(x,z,t)$. This process was repeated to obtain the filtered wall pressure over the flow domain at each time step. The time records were saved for a grid of 16 uniformly spaced streamwise locations by 16 uniformly spaced spanwise locations over the wall domain, for a total of 256 time series.

Typical methods for analysis of wall pressure were used to examine the filtered wall pressure time series data. The rms wall pressure was calculated from the mean of the square of the wall pressure for all points in the domain using

TABLE II. Resolution of the spectra.

$\Delta\omega\delta/U_\tau=0.818$	$\omega_{max}\delta/U_\tau=837.5$
$\Delta k_x\delta=0.5$	$(k_x\delta)_{max}=31.5$
$\Delta k_z\delta=1.5$	$(k_z\delta)_{max}=94.5$

2133 individual time instants. The wall pressure spectrum was found from the ensemble average of 2048-point Fourier transforms of the 256 time series using a Hanning window to prevent anomalies related to the nonperiodic conditions at the beginning and end of each time series. For larger sensors, the sensor areas for nearby sampling points in the domain overlapped substantially so that the individual spectra for each grid point were not statistically independent. This overlap reduced the effective number of records substantially increasing the random error and causing somewhat jagged spectra for large sensors. A moving average using nine equally weighted points was used to smooth the spectra,[23] resulting in a random error of 0.02, not accounting for overlap of the larger sensor areas. Even with the smoothing the spectra for larger sensors retained a somewhat jagged appearance, but using more than nine points for smoothing resulted in smearing of important landmarks in the spectra that are related to the spatial filtering.

Wave-number spectra for the spatially filtered data were calculated at the first 533 time steps and ensemble averaged for a random error[23] of 0.04. Although it would have been desirable to calculate the wave-number spectra at more time steps, computational restrictions prevented this. The wave-number spectra calculated for one particular case using 2133 time steps was nearly identical to that using 533 time steps, indicating that no errors resulted from using fewer time steps. No window was used for the calculation of the wave-number spectra, since the computational domain is periodic in both the x and z directions. The resolution and other details of the spectra are provided in Table II.

Data are presented in this paper for sensors as large as $d_+=200$ and $L_+=180$. Larger sensors were tested but two problems affected the validity of the data. First, the sensor areas for large sensors at adjacent sampling locations overlapped, resulting in large random error as noted above. Second, data obtained with a sensor that is much larger than the typical length scale of the simulation, one half-channel width, or $U_\tau\delta/\nu=180$, may not be meaningful. At the other extreme, sensors cannot be smaller than the grid resolution. Data presented for $d_+=0$ and $L_+=0$ actually correspond to the simulated wall pressure field with no filtering, so the equivalent sensor dimensions correspond to the resolution of the grid, $\Delta x_+=17.6$ by $\Delta z_+=5.9$.

Although this numerical database provides a vast set of velocity and pressure data that correspond quite well to experimental results,[17–20] the wall pressure data may not be completely representative for several reasons. First, the momentum thickness Reynolds number for the simulation, $\mathrm{Re}_\theta=280$, is lower than that achieved experimentally, although the low Reynolds number is necessary because of computational limitations. Second, periodic boundary conditions require that the fluid structures entering the computational domain be identical to those leaving the domain, which cannot occur in a real channel flow. Third, the extent of the computational domain is very limited, 2253 viscous units in the streamwise direction and 755 viscous units in the spanwise direction. Finally, the position of the centerline of the simulated channel is at a very small distance from the wall corresponding to $\delta U_\tau/\nu=180$, suggesting that contributions by the inner region of the flow may dominate because the outer flow is largely absent.[17] While these problems may make relating this wall pressure database to practical flows difficult, they do not affect the results described here. The focus in this paper is on how averaging in space by a transducer of finite size affects the frequency spectrum. While the numerical database may have some weaknesses, it still has the general character expected for a turbulent wall pressure field.[17,19,20] Furthermore, it provides the most detailed "model" to date for a wall pressure field. For this reason, the results obtained by applying wall pressure sensors of different sizes and sensitivities to this model wall pressure field should accurately reflect the character of spatial averaging that occurs when experimentally measuring the wall pressure field using transducers of finite size.

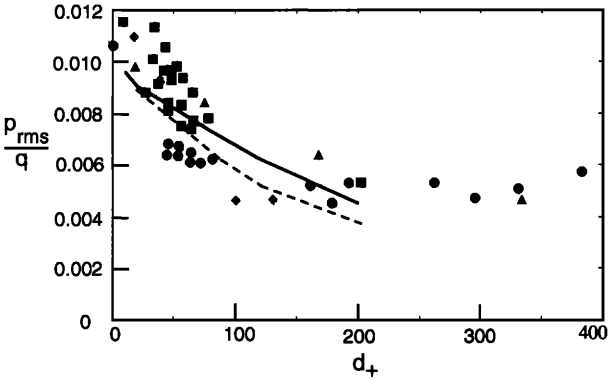

FIG. 1. The dependence of the rms wall pressure on the transducer size for circular transducers (see Refs. 5, 6, 14–16, and 24–30). ■ pinhole microphone; ▲ deflection microphone; ● piston-type microphone; ◆ unknown microphone type; ——— deflection microphone (this study); ----- piston-type microphone (this study).

II. RESULTS

Over the years many studies have provided measurements of the rms wall pressure in turbulent wall-bounded flows using circular sensors of different sizes. Figure 1 shows the rms wall pressure nondimensionalized by the dynamic pressure, $q=\rho U_{cl}^2/2$, as a function of sensor diameter for a number of studies as well as the analysis described here. Although $d^*=d_+(U_\tau/U_{cl})$ was shown to be a better scaling for the sensor diameter,[17] we use d_+ because information was not always available to determine d^*, and d_+ is the more traditional measure. Farabee and Casarella[15] showed that p_{rms}/τ_w is dependent on the Reynolds number $\mathrm{Re}_\tau=U_\tau\delta/\nu$. But nondimensionalization with q seems to reduce the sensitivity to the Reynolds number. The value of p_{rms}/q calculated in this study decreases with sensor diameter in a similar way to the experimental data in spite of the low Re_τ and $p_{rms}/\tau_w(1.54)$ in this study compared to most

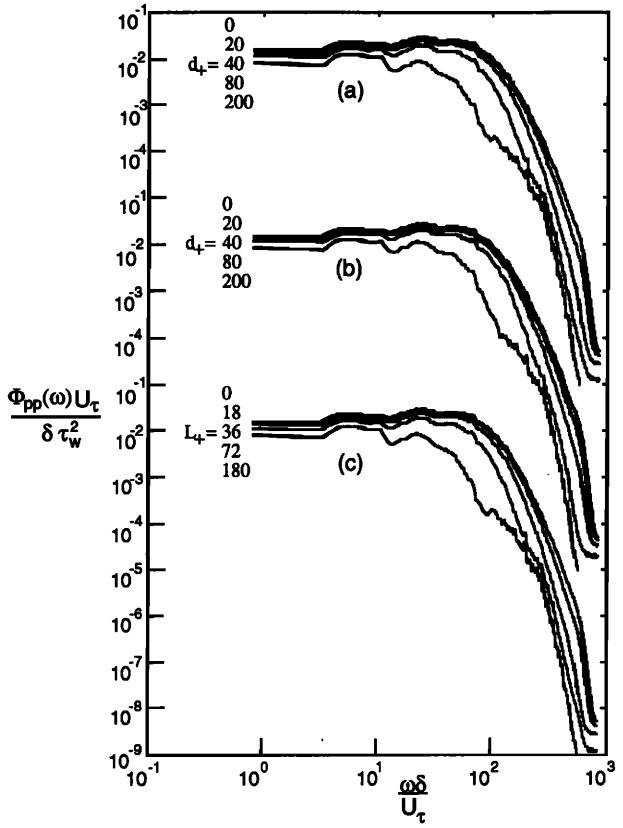

FIG. 2. Frequency spectrum of the wall pressure for (a) circular piston-type microphone, (b) circular deflection microphone, and (c) square piston-type microphone. Transducer dimensionless diameters d_+ or length of a side L_+ are noted in the figure.

experiments. A deflection-type transducer has less attenuation for a given size than a piston-type transducer because of the lower sensitivity of a deflection-type transducer near its edge compared to its center, effectively reducing its dimensions. Circular and square piston-type transducers have nearly identical attenuation of the rms pressure for the same area, a logical consequence of their uniform sensitivity and the randomness of the wall pressure field.

The amplitudes of the frequency spectra $\Phi_{pp}(\omega)$ are also reduced as the transducer increases in size for all three types of transducers as shown in Fig. 2. Several trends are notable. First, the high-frequency portion of the spectrum is increasingly attenuated as the size of the transducer increases. However, the attenuation of the spectral density is most evident for the largest transducers for $20<\omega\delta/U_\tau<150$, the middle of the range of frequencies and not at the highest frequencies. The spectral density does not drop off uniformly with frequency for the larger transducers. This is particularly evident for the largest sensors, where the slope of the spectrum changes at $\omega\delta/U_\tau\sim100$. This effect is related to the zeros appearing in the normalized wave-number response function of the sensor, described shortly.

An interesting effect of increasing transducer size is that the spectrum is attenuated even at the lowest frequencies. The common wisdom is that the detection of large-scale structures corresponding to low frequencies is unaffected unless the transducer is larger than the structure. Using the convection velocity for this pressure field,[20] structures that are larger than the largest transducer modeled in this study correspond to frequencies of $\omega\delta/U_\tau<72$. But in Fig. 2 attenuation is evident below this frequency. The low-frequency attenuation comes about from the frequency representation of a wave-number-frequency phenomenon. The frequency spectrum $\Phi_{pp}(\omega)$ can be represented as the integral over all wave numbers of the wave-number-frequency spectrum, $\Phi_{pp}(k_x,k_z,\omega)$, such that

$$\Phi_{pp}(\omega)=\int_{-\infty}^{\infty}\int_{-\infty}^{\infty}\Phi_{pp}(k_x,k_z,\omega)|H(\mathbf{k})|^2\,dk_x\,dk_z. \quad (5)$$

From (5) it is evident that the application of the spatial filtering, $H(\mathbf{k})$, will reduce the contribution of the higher wave numbers to the frequency spectrum. Since the spectral density at any particular frequency is the integrated contribution over all wave numbers, some of which are attenuated by the spatial filtering of the sensor, the spectral levels are reduced even at the lowest frequencies. Citriniti *et al.*[31] found similar attenuation of the low-wave-number portion of the turbulent velocity spectrum measured using very long hot wires and showed analytically that this is caused by representing a three-dimensional wave-number spectrum in one dimension. A less important cause of low-frequency attenuation is the elongation of pressure-producing structures in the spanwise direction.[20] Spatial averaging results when the small dimension of the structure is less than the sensor dimension.

Although the attenuation of low frequencies is readily explained, it is important to note that the low-frequency portion of the spectrum for the database may not be representative of the physical situation. The simulation used in this study had a periodic boundary condition at its inlet and outlet, so that a flow structure that leaves the flow domain at the downstream end simultaneously reenters it at the upstream end. This becomes a problem when the computational domain is not long enough for the streamwise decay of a large structure, allowing it to continually reenter the domain. Furthermore, Choi and Moin[20] found "artificial acoustics" appearing at the lowest computational wave number that may be related to the finite time step and the feedback resulting from periodic boundary conditions.

The wave-number spectrum for different size transducers is helpful in understanding the character of the frequency spectrum. The streamwise wave-number spectra $E_{pp}(k_x)$ are shown in Fig. 3. The lobed structure of the spectra is a direct result of the zeros in the normalized wave-number response function for the transducer. For instance, the first zero for a circular piston-type transducer occurs at $kr_0=3.832$. Since the energy in turbulent spectra is centered about $k_z=0$, k can be approximated by k_x. Thus for the transducer with a diameter of $d_+=200$, this zero corresponds to $k_x\delta=6.9$, where a low point appears in the spectrum for this transducer as shown in Fig. 3(a). The zeros in the wave-number spectra of the circular transducers appear only as small valleys rather than zeros for two reasons. First, the wave-number resolution is too coarse to adequately resolve the valleys related to the zeros. Second, the application of a circular transfer function to data in a rectangular grid results in some smearing of the

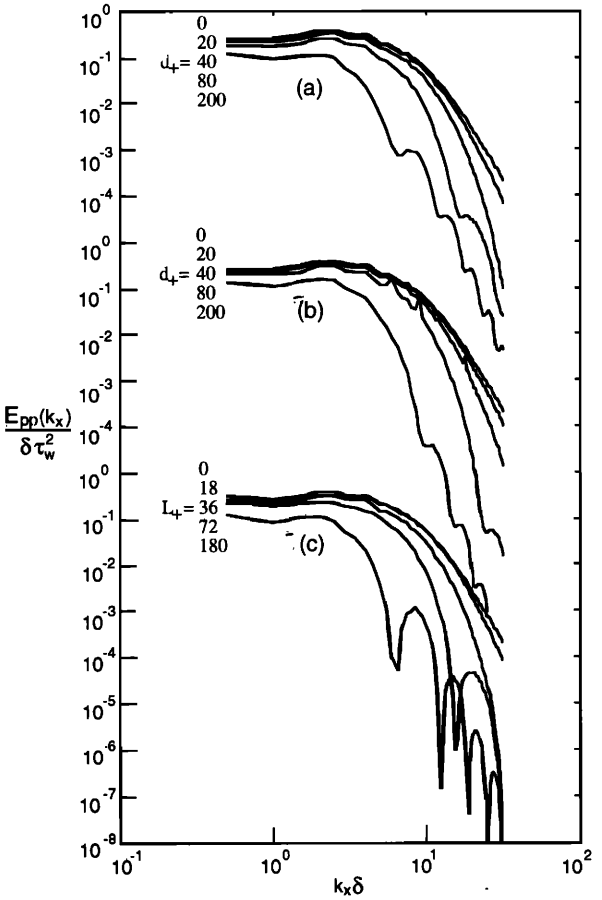

FIG. 3. Streamwise wave-number spectrum of the wall pressure for (a) circular piston-type microphone, (b) circular deflection microphone, and (c) square piston-type microphone.

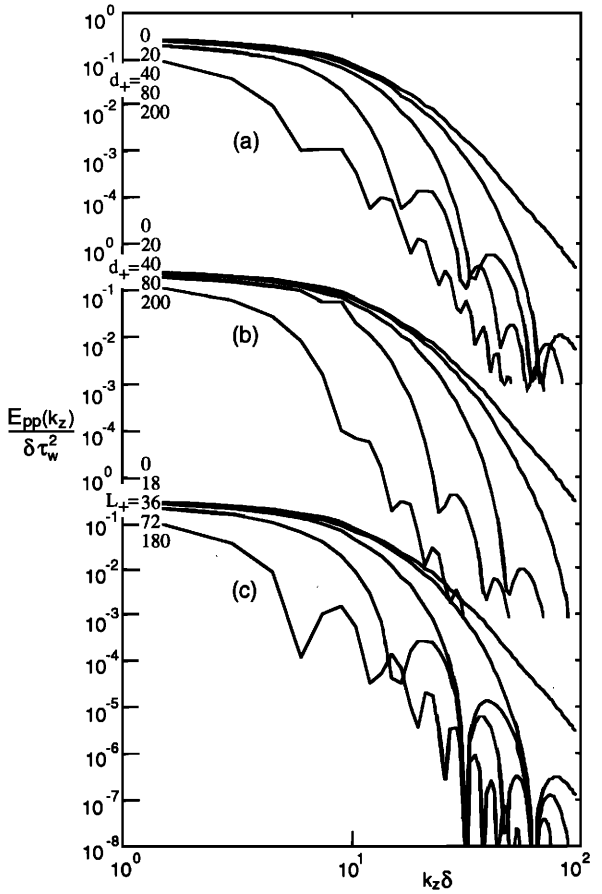

FIG. 4. Spanwise wave-number spectrum of the wall pressure for (a) circular piston-type microphone, (b) circular deflection microphone, and (c) square piston-type microphone.

spectra for the circular transducers. The zeros in the wave-number spectra are much sharper for the case of a square piston-type transducer shown in Fig. 3(c). Although the attenuation of the spectrum is related to the roll-off and zeros in the normalized wave-number response function at higher wave numbers, attenuation is evident even at low wave numbers for the largest transducers as a result of integrating a two-dimensional wave-number spectrum over the spanwise dimension.

The spatial resolution and smearing effects are even worse for the transverse wave-number spectra $E_{pp}(k_z)$, shown in Fig. 4, since the spanwise dimension of the flow domain is smaller than the streamwise dimension. For example, in the k_z-wave-number spectrum for a circular piston-type transducer, shown in Fig. 4(a), the zeros appear merely as a flattening of the wave-number spectrum. The zeros are sharper for the square transducer, shown in Fig. 4(c), but even here they are smeared because of poor wave-number resolution. As with the streamwise wave-number spectra, the attenuation of the spanwise spectra is evident at low wave numbers as well as high wave numbers.

The appearance of zeros in the k_x-wave-number spectrum that result from the zeros in the normalized wave-number response of the transducer suggests that these zeros cause the large attenuation in the middle of the range of frequencies for frequency spectra of the larger transducers in Fig. 2. An example of this attenuation occurs at $\omega\delta/U_\tau \sim 100$ in Fig. 2(a) for $d_+ = 200$. If the midrange attenuation in the frequency spectrum is simply a result of zeros in the normalized wave-number response of the transducer, then frequency spectra derived using Taylor's frozen field hypothesis should have similar attenuation to the directly calculated frequency spectra. Taylor's frozen field hypothesis requires a nondispersive relationship between the frequency and wave number such that $\omega = U_c k_x$ and $\Phi_{pp}(\omega) = E_{pp}(k_x)/U_c$, where the convection velocity of the wall pressure field is $U_c = 0.72 U_{\mathrm{cl}}$.[20] By comparing the actual frequency spectrum for this numerical database with that calculated from the wave-number spectrum, Taylor's frozen field hypothesis has been shown to accurately describe the relationship between the frequency spectrum and the wave-number spectrum when there is no spatial averaging.[20]

Applying the frozen field hypothesis to spatially filtered data is shown in Fig. 5 for three representative cases. At low frequencies the frequency spectrum derived from the wave-number spectrum using Taylor's frozen field matches the actual frequency spectrum very closely. At higher frequencies the frequency spectrum calculated from the wave-number spectrum drops below the actual frequency spectrum. When the first zero is outside of the range of frequencies, no dips in

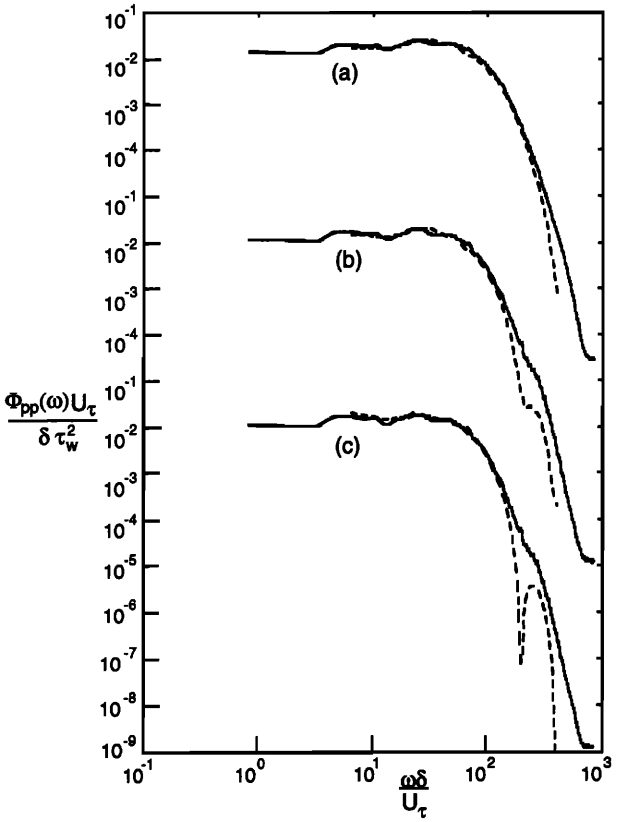

FIG. 5. Comparison of the measured frequency spectrum and the frequency spectrum calculated from Taylor's frozen field hypothesis. ——— Measured frequency spectrum; ----- spectrum from frozen field. (a) Circular piston-type microphone, $d_+=40$; (b) circular piston-type microphone, $d_+=80$; (c) square piston-type microphone, $L_+=72$.

the frequency spectrum occur. For example, the first zero for a circular piston-type transducer of $d_+=20$ occurs at $\omega\delta/U_\tau\sim880$, which is beyond the limit of frequencies measured. But for $d_+=40$ the zero occurs at $\omega\delta/U_\tau\sim440$ and the resulting roll-off in the frozen field spectrum is severe, as shown in Fig. 5(a). The zeros in the frequency spectrum calculated from the wave-number spectrum correspond to dips in the frequency spectrum for larger transducers. This is evident in Fig. 5(b) at $\omega\delta/U_\tau\sim220$, which corresponds to the zero in the corresponding wave-number spectrum for $d_+=80$ at $k_x\delta=17.2$ in Fig. 3(a). It is even more obvious in Fig. 5(c) for a square transducer at $\omega\delta/U_\tau\sim200$, which corresponds to the zero in the corresponding wave-number spectrum for $L_+=72$ at $k_x\delta=16$ in Fig. 3(c). The dips in the frequency spectra are not nearly as sharp as those in the frozen field spectra calculated from the wave-number spectrum because of smearing of the frequency spectra by imperfect convection of the pressure field.

III. CORCOS WALL PRESSURE CORRECTION

Clearly, a transducer of dimension d will have difficulty in detecting structures of frequency ω traveling at convection velocity U_c when $2\pi U_c/\omega<d$ as pointed out in several earlier analyses of the effect of transducer size on spectral measurements.[9,11,12] But the zeros in the transducer's wave-number response function provide a bound on the maximum

TABLE III. Maximum measurable frequency for different transducers.

Type of sensor	Frequency of first zero	Dimension of sensor
Square piston:	$\omega_0=2\pi U_c/L$	$L_{0+}=17$
Circular piston:	$\omega_0=7.7U_c/d$	$d_{0+}=21$
Circular deflection:	$\omega_0=11.0U_c/d$	$d_{0+}=30$

frequency that a transducer of a particular size can measure. The maximum frequency that a transducer can measure can be related to the first zero in the transducer's wave-number response function by using Taylor's frozen field hypothesis, $k_x=\omega/U_c$. Now consider the wave number k_0 corresponding to the first zero for a circular piston-type transducer, which is at $k_0r_0=3.832$ or $k_0d=7.664$. Since most of the energy in turbulent spectra is centered about $k_z=0$, k can be approximated by k_x. Thus the wave number of the first zero can be rewritten in terms of frequency as $k_0d\approx(\omega_0/U_c)d\approx7.7$. Rearranging, the frequency corresponding to the first zero of the transducer is $\omega_0\approx7.7U_c/d$. Expressions for the frequencies of the first zero for the types of transducers in this study are indicated in Table III. Of course, attenuation in the measured spectrum should be expected even for frequencies less than ω_0, because of the roll-off of the normalized wave-number response function.

The frequency of the first zero ω_0 should be greater than the maximum measured frequency $\omega_{\max}$ for accurate measurement of the wall pressure spectrum. Setting $\omega_{\max}$ equal to ω_0 results in a relation for the largest size of transducer that can be used without exceeding the first zero in the normalized wave-number response. The sensor dimensions found in this way for this numerical database are shown in Table III. The diameter of a circular piston-type transducer corresponding to the first zero for this study is $d_{0+}=21$. For a circular deflection-type transducer, the diameter is $d_{0+}=30$. In fact, the values for which the rms wall pressure begins to deviate substantially from the true value in Fig. 1 corresponds to these diameters.

When $d_+\geqslant40$ and $L_+\geqslant36$, so that $\omega_0<\omega_{\max}$, the spectra fall substantially short of the true spectrum at high frequencies as shown in Fig. 2. The same result is evident in the data of Schewe.[16] Table IV indicates the values for f_0 and $f_{\max}$ for the different sized transducers that he used. For the three smallest transducers the frequency of the first zero f_0 was larger than the maximum measured frequency $f_{\max}$ and the wall pressure spectra collapsed when the Corcos correction[3] was applied in Schewe's Fig. 12.[16] However, for the two largest transducers, the spectra fell well below those for the smaller transducers at the highest frequencies even

TABLE IV. Spatial resolution for Schewe's data (see Ref. 16).

d_+	$f_0=\omega_0/2\pi$	$f_{\max}=\omega_{\max}/2\pi$ (plotted in Schewe's Fig. 12)
19	5880	1250
39	2800	1600
75	1470	1250
168	650	800
333	330	400

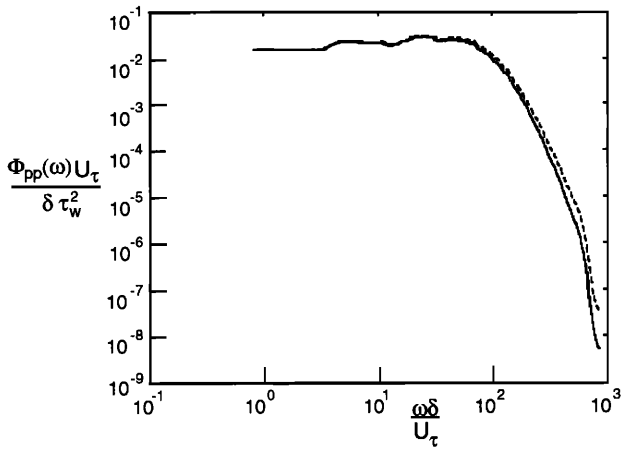

FIG. 6. Comparison of the Corcos corrected spectrum (true spectrum) with uncorrected spectrum. ----- True spectrum; ——— uncorrected spectrum.

when the Corcos correction was applied, because $f_{max}>f_0$.

To further test the effectiveness of the Corcos correction,[3] we applied it to the spectra calculated from the numerical database. The Corcos correction expresses the ratio of the measured spectral density to the true spectral density, Φ_m/Φ, as a function of $\omega r_0/U_c$ or $\omega L/U_c$. For the purposes of this study Corcos' tabulated data was fitted to a polynomial curve. For a circular piston transducer, a tenth-order polynomial was used for $0\leqslant\omega r_0/U_c\leqslant 4.514$ and a third-order polynomial was used for $4.514\leqslant\omega r_0/U_c\leqslant 10$. For a square piston transducer, a tenth-order polynomial was used for the entire frequency range, $0\leqslant\omega L/U_c\leqslant 10$.

The Corcos correction was first applied to the data for which no spatial filtering was used, denoted as $d_+=0$ here, because even the unfiltered data with a grid resolution of $\Delta x_+=17.6$ by $\Delta z_+=5.9$ should have some attenuation from spatial averaging. The correction that was applied was based on a square transducer with an identical area, since the Corcos correction is tabulated only for circular and square transducers. The corrected spectrum, which is called the "true spectrum," is shown in Fig. 6. Using the correction for a circular transducer of the same area provided results that were nearly identical. This is not surprising since when the Corcos correction is converted to area instead of radius or length of a side, the correction for square and circular transducers are within 1% or 2% of each other.

Representative spectra after the application of the Corcos correction are shown in Fig. 7. At low frequencies the Corcos correction does not entirely account for the attenuation, although it brings the corrected spectra closer to the true spectra than with no correction. For a range of frequencies greater than about $\omega\delta/U_\tau\sim 20$ the corrected spectra nearly match the true spectrum. Nevertheless, at higher frequencies the corrected spectra rise above the true spectrum.

The inability of the Corcos method to adequately correct the low-frequency portion of the spectrum may be related to the nature of the computationally derived wall pressure field and not to the Corcos correction. Choi and Moin[20] showed that similarity functions based on the Corcos separation of variables representation of the wall pressure spectra do not

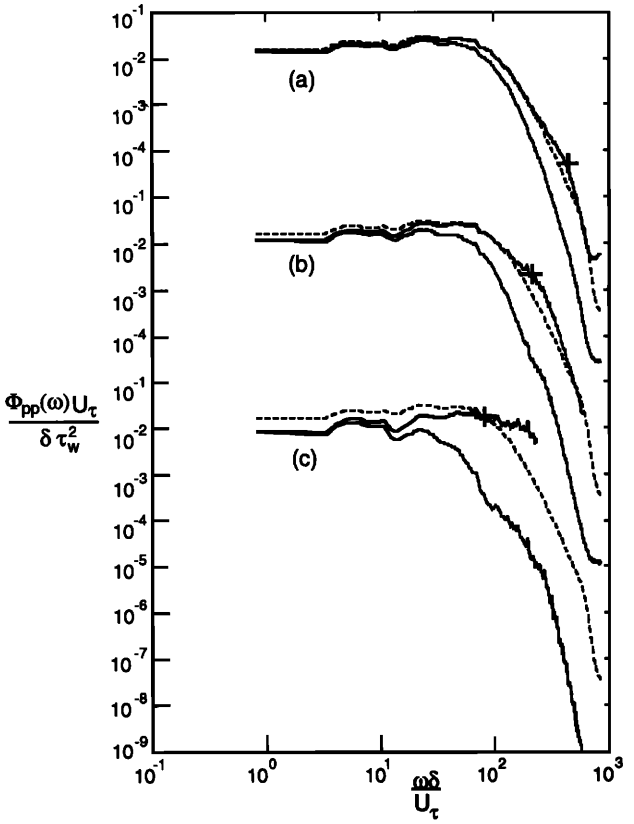

FIG. 7. The Corcos correction applied to three piston-type circular sensors. (a) $d_+=40$; (b) $d_+=80$; (c) $d_+=200$. The lower solid curve is the uncorrected spectrum. The upper solid curve is the corrected spectrum. The dashed curve is the true spectrum. The frequency corresponding to the first zero is marked with a + on the corrected spectra.

collapse, indicating that the functions are not self-similar for the computational database. Furthermore, Keith *et al.*[17] noted that the wall pressure frequency spectra based on the computational database have lower than expected spectral levels at low frequencies, possibly due to small contributions from the outer region.

Although Corcos tabulated his correction for $0\leqslant\omega r_0/U_c\leqslant 10$, the frequency of the first zero of the normalized wave-number response function bounds the application of the correction. For instance, Table III indicates that the frequency of the first zero for a circular piston transducer occurs at $\omega_0\approx 7.7U_c/d$, or $\omega_0 r_0/U_c\approx 3.8$. Thus the Corcos correction should only be used for $0\leqslant\omega r_0/U_c\leqslant 3.8$ for circular transducers. A similar analysis leads to a bound of $0\leqslant\omega L/U_c\leqslant 6.3$ for square transducers. The position of the frequency corresponding to this limit is marked with a + along the corrected spectra in Fig. 7. No + appears along the true spectrum because the maximum frequency encountered corresponded to $\omega L/U_c=3.70$, within the bounds for a square transducer.

The + appears at the location in the corrected spectrum where it deviates substantially from the true spectrum. Although the appearance of zeros in the normalized wave-number response function of the transducer results in attenuating the spectrum, the Corcos correction appears to overcompensate for this effect. This is not related to the data

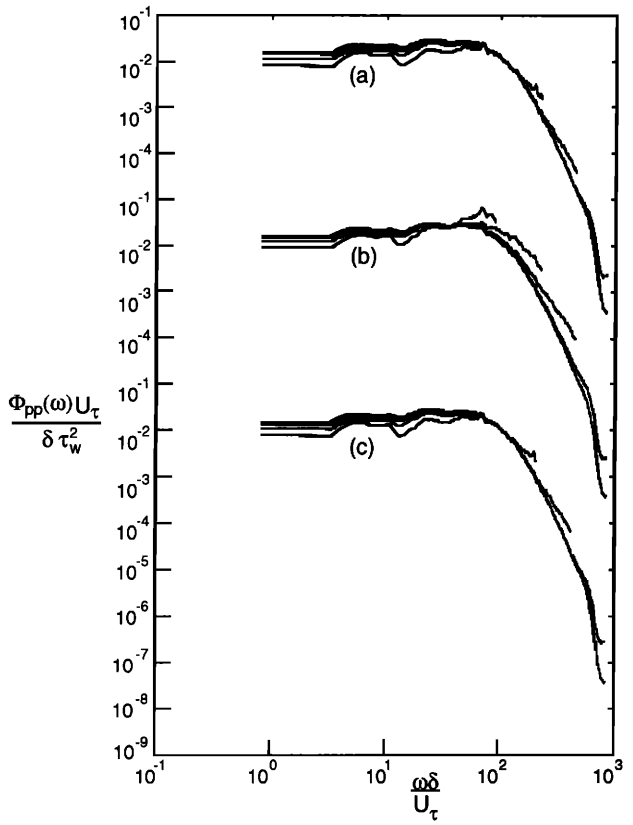

FIG. 8. Corrected frequency spectra for (a) circular piston-type microphone, (b) circular deflection microphone, and (c) square piston-type microphone. Curves correspond to those of Fig. 3. Each curve can be identified from its high-frequency limit, which decreases with transducer size. For the largest piston-type transducer, the high-frequency limit occurs at $\omega d/U_\tau \sim 85$ and is hidden by the other curves in (a) and (c).

of Willmarth and Wooldridge[5] upon which Corcos based his correction, since the data did not exceed the bound on frequency listed in Table III. It is difficult to pinpoint the cause of the overestimation of the Corcos correction at high frequencies. It may have resulted from errors in the experimental data that Corcos used, the curve fit to that experimental data, or the numerical integration used to obtain the tabulated results. In any case, the range of frequencies for which the Corcos correction overpredicts the true spectrum corresponds to a frequency range for which the correction probably should not be used anyway because of zeros in the normalized wave-number response function of the transducer.

The Corcos corrected spectra corresponding to the spectra in Fig. 2, as limited by the bound related to the first zero in the response function, are shown in Fig. 8. Consider the Corcos correction for a circular piston transducer, shown in Fig. 8(a). Clearly, the Corcos correction inadequately accounts for the attenuation below a frequency of $\omega\delta/U_\tau \sim 65$, although this may be related to the character of the database itself and not to the Corcos correction. Above this frequency, the corrected spectrum follows the true spectrum quite well, until the frequency nears the first zero cutoff where the corrected spectrum rises above the true spectrum. Although the Corcos correction was intended for sensors with a uniform response, it appears to work reasonably well for circular deflection transducers as shown in Fig. 8(b). The corrected spectra are closer to the true spectrum than uncorrected spectra in Fig. 2(b), but the Corcos method overcorrects as $\omega r_0/U_c$ nears its limit at high frequencies. Applying the Corcos correction to the data for a square piston-type transducer produces similar results to that for a circular piston-type sensor as shown in Fig. 8(c).

IV. CONCLUSIONS

The attenuation of the wall pressure spectrum resulting from the spatial averaging over the face of the wall pressure transducer has two causes. The first cause is attenuation resulting from the appearance of zeros in the wave-number spectrum related to the lobed structure of the normalized wave-number response function $H(\mathbf{k})$. Although the zeros are smeared when the frequency spectrum is considered, they can greatly reduce the spectral density at higher frequencies. To avoid the effect of zeros on the measured frequency spectrum, the highest measured frequency ω_{max} should be less than the frequency of the first zero ω_0. This results in the simple, approximate relationship that

$$\omega_{max} d/U_c < C, \tag{6}$$

where C is 2π, 7.7, and 11.0 for square piston (d is replaced by L), circular piston, and circular deflection microphones, respectively. The second cause of attenuation is the simple reduction in the spectral density due to integrating a wave-number-frequency spectrum over the spatially filtered wave-number domain, Eq. (5). This attenuation is not nearly as severe as that due to the appearance of zeros. The Corcos correction provides a good estimate of the true wall pressure spectrum up to the limit of (6).

ACKNOWLEDGMENTS

Thanks to Dr. Joao Neves of the Naval Research Laboratory for providing code to access the direct simulation database used in this study, and to Dr. Robert Moser of NASA-Ames and Dr. Parviz Moin of Stanford University for providing the database for our use. Dr. David Hurdis, Naval Undersea Warfare Center, New London, CT, made this research possible. Dr. William Keith and Bruce Abraham provided many helpful comments during the course of this work. A portion of this work was performed while the author was on leave to the Naval Undersea Warfare Center, New London, CT. Part of this work was funded the Office of Naval Research under Contract No. N0014-89-J-1439, Mr. James A Fein, Program Manager.

[1] W. K. Blake, *Mechanics of Flow-Induced Sound and Vibration, Vol. II: Complex Flow-Structure Interactions* (Academic, Orlando, 1986), pp. 569–573.

[2] G. M. Corcos, J. W. Cuthbert, and W. A. Von Winkle, "On the measurement of turbulent pressure fluctuations with a transducer of finite size," Univ. of California Inst. of Eng. Res. Rep., Ser. 82, No. 12 (Nov. 1959).

[3] G. M. Corcos, "On the resolution of pressure in turbulence," J. Acoust. Soc. Am. **35**, 192–199 (1963).

[4] G. M. Corcos, "The resolution of turbulent pressures at the wall of a boundary layer," J. Sound Vib. **6**, 59–70 (1967).

[5] Corcos[3] references a Willmarth and Wooldridge report for the experimental basis of his correction that this author could not obtain. But based on a discussion in Ref. 6, the information in the report is the same as that in W. W. Willmarth and C. E. Wooldridge, "Measurements of the fluctuating

pressure at the wall beneath a thick turbulent boundary layer," J. Fluid Mech. **14**, 187–210 (1962); corrigendum, J. Fluid Mech. **21**, 107–109 (1965).
[6] W. W. Willmarth and F. W. Roos, "Resolution and structure of the wall pressure field beneath a turbulent boundary layer," J. Fluid Mech. **22**, 81–94 (1965).
[7] W. L. Keith and J. C. Bennett, "Correction of wall pressure fluctuation measurements with a view to hydrodynamic applications," The Forum on Turbulent Flows, ASME–JSME Fluids Engineering Conference, Portland, Oregon, 24–28 June 1991 (reprinted as NUSC Reprint Report 8889, 1 July 1991).
[8] P. H. White, "Effect of transducer size, shape, and surface sensitivity on the measurement of boundary-layer pressures," J. Acoust. Soc. Am. **41**, 1358–1363 (1967).
[9] G. J. Kirby, "The effect of transducer size, shape and orientation on the resolution of boundary layer pressure fluctuations at a rigid wall," J. Sound Vib. **10**, 361–368 (1969).
[10] R. B. Gilchrist and W. A. Strawderman, "Experimental hydrophone-size correction factor for boundary-layer pressure fluctuations," J. Acoust. Soc. Am. **38**, 298–302 (1965).
[11] D. M. Chase, "Turbulent-boundary-layer pressure fluctuations and wave-number filtering by nonuniform spatial averaging," J. Acoust. Soc. Am. **46**, 1350–1365 (1969).
[12] J. E. Ffowcs-Williams, "Boundary-layer pressures and the Corcos model: A development to incorporate low-wavenumber constraints," J. Fluid Mech. **125**, 9–25 (1982).
[13] F. E. Geib, "Measurements on the effect of transducer size on the resolution of boundary-layer pressure fluctuations," J. Acoust. Soc. Am. **46**, 253–261 (1968).
[14] M. K. Bull and A. S. W. Thomas, "High frequency wall-pressure fluctuations in turbulent boundary layers," Phys. Fluids **19**, 597–599 (1976).
[15] T. M. Farabee and M. J. Casarella, "Spectral features of wall pressure fluctuations beneath turbulent boundary layers," Phys. Fluids A **3**, 2410–2420 (1991).
[16] G. Schewe, "On the structure and resolution of wall-pressure fluctuations associated with turbulent boundary-layer flow," J. Fluid Mech. **134**, 311–328 (1983).
[17] W. L. Keith, D. A. Hurdis, and B. M. Abraham, "A comparison of turbulent boundary layer wall pressure spectra," J. Fluids Eng. **114**, 338–347 (1992). Also see "A comparison of turbulent boundary layer wall-pressure spectra," in NCA-Vol. 11/FED-Vol. 130, *Flow Noise Modeling, Measurement, and Control*, edited by T. M. Farabee, W. L. Keith, and R. M. Lueptow (ASME, New York, 1991), pp. 1–19.
[18] J. Kim, P. Moin, and R. Moser, "Turbulence statistics in fully developed channel flow at low Reynolds number," J. Fluid Mech. **177**, 133–166 (1987).
[19] J. Kim, "On the structure of pressure fluctuations in simulated turbulent channel flow," J. Fluid Mech. **205**, 421–451 (1989).
[20] H. Choi and P. Moin, "On the space-time characteristics of wall-pressure fluctuations," Phys. Fluids A **2**, 1450–1460 (1990).
[21] A. V. Smol'yakov and V. M. Tkachenko, *The Measurement of Turbulent Fluctuations: An Introduction to Hot-Wire Anemometry and Related Transducers* (Springer-Verlag, Berlin, 1983), pp. 147–174.
[22] H. M. Fitzpatrick, "Spatial resolution effected by a recessed microphone," J. Acoust. Soc. Am. **40**, 1247 (1966).
[23] D. E. Newland, *An Introduction to Random Vibrations and Spectral Analysis* (Longman Scientific and Technical, Essex, 1984), pp. 116, 137–138, 224.
[24] J. A. Astolfi, P. Bally, A. Fages, and B. E. Forestier, "Relation between wall-pressure fluctuations and a large instantaneous velocity gradient $\partial U/\partial y$ beneath a turbulent boundary layer," Eur. J. Mech. B/Fluids **11**, 573–586 (1992).
[25] W. K. Blake, "Turbulent boundary-layer wall-pressure fluctuations on smooth and rough walls," J. Fluid Mech. **44**, 637–660 (1970).
[26] See National Technical Information Service Document N73-33177/9 (Max-Planck-Institut fur Stromungsforschung Rep. No. 9/1973, R. Emmerling, 1973, "The instantaneous structure of the wall pressure under a turbulent boundary layer"). Copies may be ordered from the National Technical Information Service, Springfield, Virginia, 22161. Berichte Nr. 9, Max-Planck-Institut fur Stromungsforschung, 1973.
[27] A. V. Johansson, J.-Y. Her, and J. H. Haritonidis, "On the generation of high-amplitude wall-pressure peaks in turbulent boundary layers and spots," J. Fluid Mech. **175**, 119–142 (1987).
[28] C. C. Karangelen, V. Wilczynski, and M. J. Casarella, "Large amplitude wall pressure events beneath a turbulent boundary layer," in NCA-Vol. 11/FED-Vol. 130, *Flow Noise Modeling, Measurement, and Control*, edited by T. M. Farabee, W. L. Keith, and R. M. Lueptow (ASME, New York, 1991), pp. 45–54.
[29] G. C. Lauchle and M. A. Daniels, "Wall-pressure fluctuations in turbulent pipe flow," Phys. Fluids **30**, 3019–3024 (1987).
[30] H. H. Schloemer, "Effects of pressure gradients on turbulent-boundary-layer wall-pressure fluctuations," J. Acoust. Soc. Am. **42**, 93–113 (1967).
[31] J. H. Citriniti, D. Ewing, and W. K. George, "Long hot-wires and the measurement of large scale turbulent fluctuations," in FED-Vol. 183, Fluid Measurement and Instrumentation, edited by T. B. Morrow, G. L. Morrison, and R. A. Gore (ASME, New York, 1994), pp. 45–52.